Astronomy & Astrophysics manuscript no. chapter2
November 30, 2017

Solar wind and CME influence on the magnetosphere

Impact estimations derived from empirical correlations between in situ solar-wind measurements and the geomagnetic *Kp* index

M. S. Venzmer

University of Goettingen, Institute for Astrophysics, Friedrich-Hund-Platz 1, 37077 Göttingen, Germany

First draft 28 April 2017; received date; accepted date

ABSTRACT

Context. Variations in the Earth's magnetosphere are largely evoked by influence through the solar wind. These magnetospheric disturbances have diverse effects on the terrestrial environment. Especially the effects of severe geomagnetic storms created by coronal mass ejections (CMEs) pose various threats to sensitive technical systems and exposed humans. Thus, the development of quantitative forecasts for magnetospheric impacts caused by solar wind and CMEs is very important.
Aims. This study's goals are to estimate the magnetospheric impact from solar activity in general, from solar wind and also to predict it for CMEs in particular. We present empirical dependencies between specific solar-wind parameters and the magnetospheric disturbance index *Kp*. These dependencies allow to nowcast the *Kp* index from upstream (L1) solar-wind in situ measurements. Hence, also the magnetospheric impact of CMEs is estimated solely based on their arrival velocities, predicted from coronagraphic observations. The prediction of solar-wind stream velocities from coronal hole (CH) observations, enables to estimate their impact as well.
Methods. First, we estimate the long-term variations of the yearly average *Kp* values, which are contributed by solar activity. This is achieved via logarithmic fitting of a yearly sunspot number (SSN) dependency. For the *Kp* nowcast from general solar-wind conditions, we use a correlation with the product of the parameters velocity and magnetic field z-component in GSM coordinates (vB_z). For the *Kp* forecast from estimated CME and stream velocities, we furthermore filter the solar-wind data using flagged CME times from the solar-wind structures (SWS) list provided by Richardson & Cane (2012). The solar-wind data considered in our analyses consists of 35 years (1981–2016) of high-resolution minutely OMNI data, which is composed of multi-spacecraft intercalibrated in situ measurements from 1 au. We evaluate various data processing methods and choose the methods resulting in the highest correlation coefficients with *Kp*. We analyze the *Kp* frequency distributions with respect to the depending parameters vB_z and velocity, derive their mean *Kp* per interval and further compile functional dependencies via logarithmic fitting.
Results. The obtained functional relations enable us to empirically estimate the mean *Kp* impact from measured solar activity, in situ solar wind, and remotely observed CHs and CMEs.

Key words. solar wind – sun: coronal mass ejections (CMEs) – earth

Contents

1. Introduction

It is long known (since the early 19th century) that variations in the solar wind evoke disturbances in the magnetosphere (Bartels 1962). Especially strong disturbances, called geomagnetic storms, can be provoked by coronal mass ejections (CMEs), which are embedded within the solar wind. The causes of the strongest geomagnetic storms are the compression of the solar-wind magnetic field lines within the CME shock front and the enhanced field strenghts of magnetic clouds, which are enclosed in CMEs (Bothmer 1993).

These strong geomagnetic disturbances are a threat to sensitive technical systems and exposed humans. Therefore it is important to know when magnetospheric disturbances will occur and how large they will become.

which index to use? - the *Kp* index is designed for...
More detailed information on the *Kp* index can be found in

Section basics kp...

current comparable *Kp* forecast models take into account... Elliott et al. (2013): The *Kp* index and solar-wind speed relationship: Insights for improving space weather forecasts

differences to existing studies:
here we show...
With our results presented here, we elaborate the step from the predicted CME and stream velocities to the forecast of the possible impact strength on the Earth's magnetosphere.
We make an empirical correlation of the solar-wind speed with the geomagnetic *Kp* index to obtain the capability to forecast *Kp* values solely based on the predicted CME and stream velocities. The derived functional dependencies can be used to nowcast/forecast the *Kp* index.

In situ measurements of solar wind are made almost continuously (e.g., at the first Lagrange point (L1)) in front of the magnetosphere. Since 1963 several spacecraft collected more than 50 years of data. The latest spacecraft, e.g., Wind, ACE and DSCOVR (launched in early 2015), provide real-time solar-wind data online[1] [2] [3]. These solar-wind real-time data are used to nowcast various effects on the Earth's magnetosphere, e.g., the position of the magnetospheric bow shock in front of the Earth, the magnitude of geomagnetic disturbances (e.g., *Kp* index), the positions of the polar auroral ovals, the variation of the total electron content (TEC) of the ionosphere, and the positional error of global navigation satellite systems (GNSS).

Coronal holes are the origin of the fast solar wind; their area on the solar disk, seen in EUV wavelengths, correlates with the measured velocity of solar-wind streams (Vršnak et al. 2007). This relation is used to predict the Earth-arrival velocity of solar-wind streams about 4 days in advance (Rotter et al. 2012), as is done in real-time within the empirical solar wind forecast (ESWF) at the University of Graz[4].

The velocity and the direction of CMEs can be determined in their early near-Sun stages via remote tracking with coronagraph white-light observations. Using these parameters as input for CME propagation models, their possible arrival time and arrival velocity at Earth can be derived.

For the analyses performed and found in this paper, our objectives are to estimate the magnetospheric impact of solar wind and to predict it for CMEs in particular. In Sect. 2 we determine the magnitudes of the long-time *Kp* changes due to solar activity and measure the extent of seasonal variations stemming from the Earth's orbit. To nowcast the *Kp* index, we quantify the solar-wind influence on *Kp* by deriving a functional relation with the product of solar-wind velocity and magnetic field z-component (Sect. 3). Finally, to enable *Kp* forecasts from remote observations, we estimate the *Kp* impact coming from solar wind and CMEs separately by deriving functional dependencies with their velocities (Sect. 4).

[1] Wind real-time data website: `https://pwg.gsfc.nasa.gov/windnrt/`
[2] ACE real-time data website: `http://www.swpc.noaa.gov/products/ace-real-time-solar-wind`
[3] DSCOVR real-time data website: `http://www.swpc.noaa.gov/products/real-time-solar-wind`
[4] ESWF website: `http://swe.uni-graz.at/index.php/services/solar-wind-forecast`

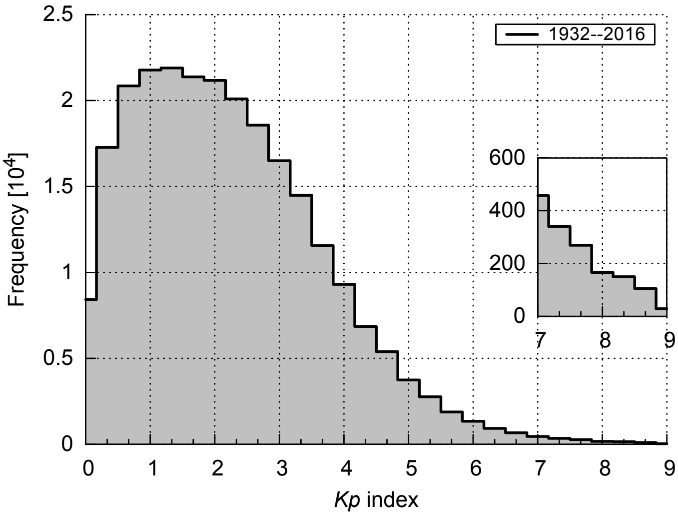

Fig. 1. *Kp* frequency distribution for the time period 1932–2016. *Kp* data from the GFZ Potsdam.

2. Long-term variations of the *Kp* index

2.1. Kp data

The *Kp* data is obtained from the GFZ Potsdam[5], where the index is now maintained. The data used in this analysis covers the time period 1932–2016.

The *Kp* frequency distribution for the time period 1932–2016 shows that the highest frequencies occur around low *Kp* values of 1+ and to higher *Kp* values the frequencies seem to decline exponentially (see Fig. 1). A *Kp* value of 9o occurred only 29 times in this time interval.

2.2. Kp variations with solar activity

solar activity is tracked with the sunspot number (SSN); SSN data
The general *Kp* distribution, seen before in Fig. 1, averages over solar activity. With different states of solar activity the *Kp* frequency distributions' shape varies. This can be seen from the yearly distributions, sorted and colored by yearly SSN (see Fig. 2). The distribution's peak position scales with SSN, that is, a high yearly SSN results also in more large *Kp* values.

The time series of yearly average *Kp* values in the time span 1932–2016 shows an imprint of the solar cycles (see the top graphs in Fig. 3). The *Kp* pattern follows the solar cycle minima and maxima as well as the changes in magnitude between solar cycles. The yearly mean *Kp* shifts about 1 unit for both variations.

As expected, the *Kp* index correlation with solar activity shows an 11-year period (see bottom graph in Fig. 3). The highest correlation coefficient 0.60 is found with a time lag of −1 year, that is, the yearly average *Kp* follows the SSN of the previous year.

cause are CHs, see paper...

[5] GFZ Potsdam website: `http://www.gfz-potsdam.de/de/kp-index/`

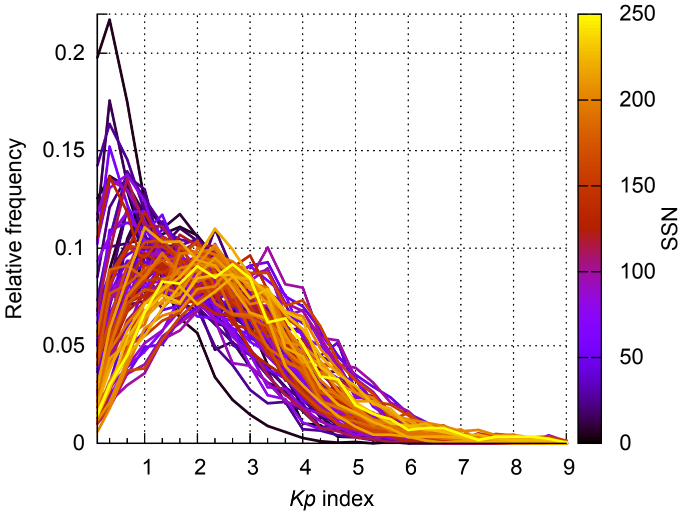

Fig. 2. Yearly *Kp* frequency distributions of the period 1932–2016 sorted and colored by SSN. *Kp* data from the GFZ Potsdam and the yearly SSN from the SILSO World Data Center.

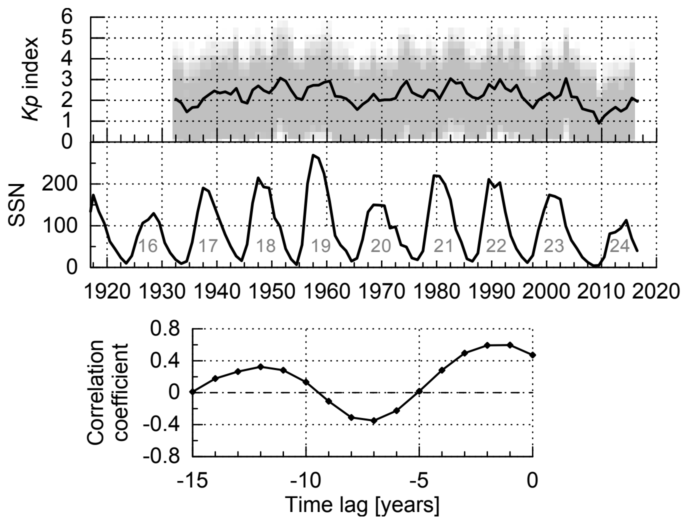

Fig. 3. Yearly *Kp* index from GFZ Potsdam and yearly SSN from the SILSO World Data Center (1932–2016) with cycle number (top). The correlation coefficients with the yearly SSN are calculated for time lags back to -15 years (bottom).

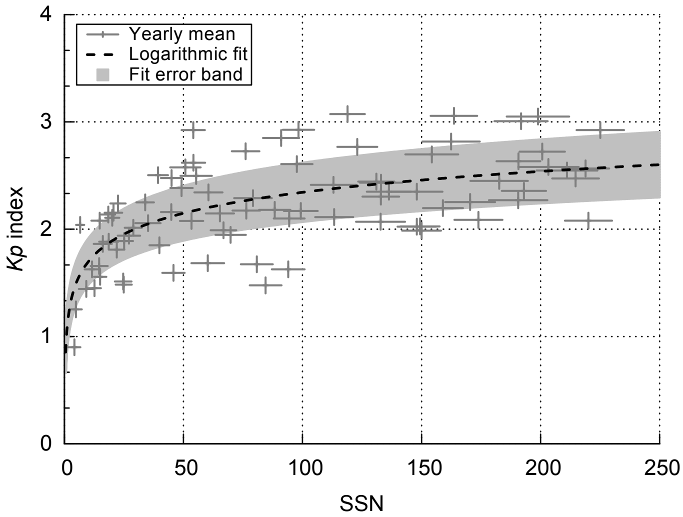

Fig. 4. Yearly mean *Kp* index over 1-year lagged SSN (+) with the weighted logarithmic fit (dashed). The error bars denote the SSN standard deviation and the relative weight from the yearly data coverage. The shaded area represents the fit error band derived from the estimated standard deviations of the fit parameters. The function (1) is used for the weighted fit. The yearly *Kp* mean values are obtained from GFZ Potsdam data and the yearly SSN from the SILSO World Data Center.

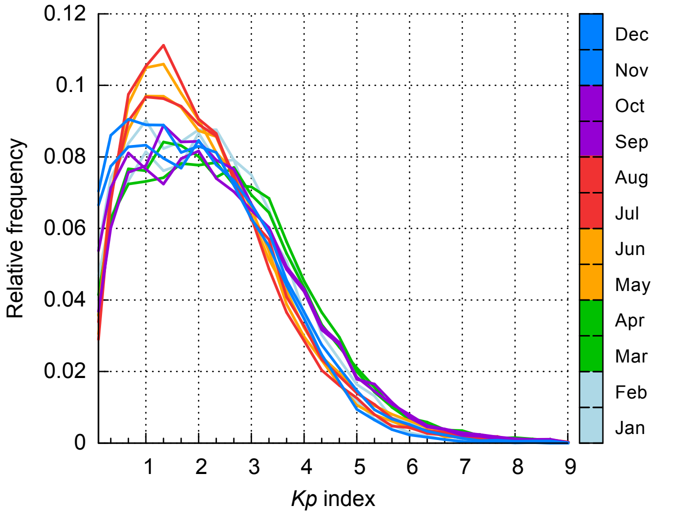

Fig. 5. Monthly *Kp* frequency distributions colored by months of the year. *Kp* data of the time period 1932–2016 from the GFZ Potsdam.

The yearly mean *Kp* indices with respect to the 1-year lagged SSN show a raise in *Kp* with increasing SSN, which is seen in Fig. 4.

We perform a fit to obtain an analytical relation for this dependency. *Kp* itself is a quasi-logarithmic index, so it is apparent to use a logarithmic fit function:

$$f(x) = a \cdot \ln(x) + b\,. \tag{1}$$

The fitted parameter values are $a = 0.281(43)$ and $b = 1.05(19)$ and lead to the relation

$$Kp(ssn) = 0.28 \cdot \ln(ssn) + 1.1\,. \tag{2}$$

In the fit result, plotted in Fig. 4, the mean *Kp* is 1.05(19) for a SSN of 1 and 2.53(30) for a SSN of 200. The fit error band has a width of about half a *Kp* unit.

2.3. Seasonal Kp variations

There also are seasonal variations in the magnetospheric disturbances. Looking at the monthly *Kp* frequency distributions for different seasons of the year, it is apparent that in the months May–August the *Kp* peak frequency is higher than in the rest of the year (see Fig. 5). In March/April and September/October the *Kp* values > 3 are more abundant.

These seasonal *Kp* changes arise from seasonal variations of the solar-wind parameters at Earth, which stem from Earth's yearly changes in orbital distance and heliographic latitude (as discussed in Sect. XX of MVVB-Paper). Another seasonal effect comes from the Earth's rotation axis tilt (±23.44°) (obliquity to the ecliptic), which changes the direction of the Earth's magnetic dipole axis to the Sun over the year (see bottom panel of Fig. 6). The rate of magnetic reconnection between solar wind and magnetosphere depends on both fields' direction to

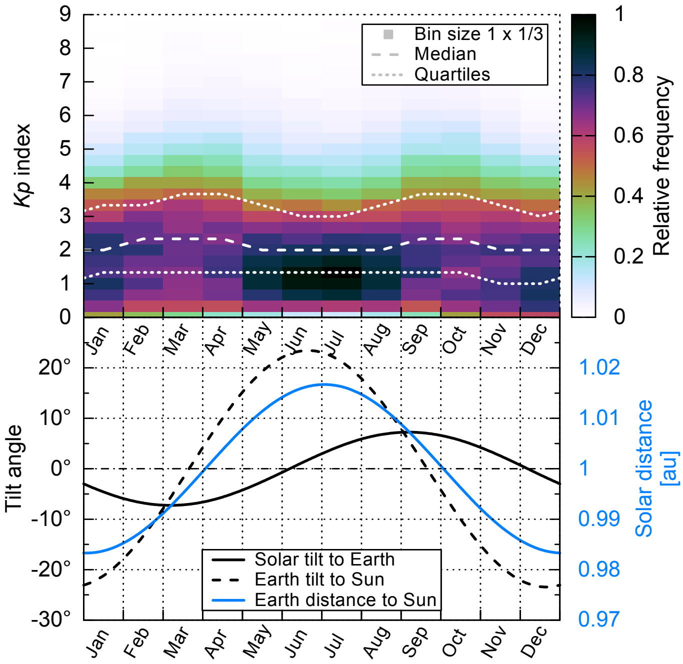

Fig. 6. *Kp* frequency distributions by month for the time period 1932–2016 with median and quartile values (top). Solar tilt angle to Earth, Earth tilt angle to Sun and Earth distance to Sun are approximated with trigonometric fuctions (bottom). switch panels...

each other (parallel/antiparallel) (see Figure in Basics...).

Kp seasonal variation effects from seasonal changing Sun tilt, Earth tilt and Earth distance.
causes (see citetRangarajan1997 p. 1282 and mention Bartels1963 too):
- Earth's rotation axis tilt (±23.44°) (obliquity to orbit/inclination of equator)
- solar rotation axis tilt (±7.25°) (cite 'NASA Earth fact sheet')
- Earth's varying solar distance of ±1.67 %
read Bothmer1998 Ch 3...

We quantify the magnitude of these effects. *Kp* frequency distributions by month, see Fig. 6.
for high *Kp* values (> 4?) there are yearly frequency maxima at the equinoxes and minima at the solstices. this variation amounts to more than 1? *Kp* unit...

The magnitudes of the SSN variation *Kp*(*ssn*) and the seasonal variation *Kp*(month) are of a similar order...?

Both variations are an indirect influence through solar wind (see paper).

3. *Kp* nowcast from in situ solar-wind measurements

3.1. Solar wind-magnetosphere coupling

The coupling between the solar wind and the magnetosphere is governed by reconnection and compression of the magnetic field lines (see Basics...).

the dayside reconnection is asymmetric

To describe this, some coupling functions with different complexity were proposed (Newell, cites? and list).

dayside reconnection:
"E_y is the rate at which southward magnetic flux is convected to the magnetosphere by the solar wind ($-v_x \cdot B_z$) in GSM coordinates," (Russell 2007)

the product of the proton velocity v and the magnetic field z-component in geocentric solar magnetospheric (GSM) coordinates B_z:

$$?checkvectors E_y = -v_x \times B_z \,(\mathrm{GSM}) \tag{3}$$

If not specified otherwise, B_z is always meant to be in GSM coordinates hereafter.

argue for vB_z:
- 3hmin(vB_z) performs in rank correlation slightly better than the sophisticated Newell formula. really?
- simple to calculate
- ...

We settle for vB_z as the coupling function to analyze.

It also is known that the solar-wind velocity itself already correlates strongly with the *Kp* index. In fact Machol et al. (2013) even proposed a linear function of the *Kp* index as a best proxy for corrupted real-time velocity measurements made by the Advanced Composition Explorer (ACE) spacecraft.

3.2. Data set, data processing and correlation

The *Kp* time series started in 1932 when there were no spacecraft to measure in situ solar wind. Thus, the surveyed time range is defined by the available in situ solar-wind data. The OMNI data set collects the longest continuous solar-wind measurements at 1 au, it covers hourly data since 1963; 5-minute and minutely data since 1981.

why this data set? - because of long time coverage, to magnetospheric bow shock calculated solar wind and integrated geomagnetic indices (see Paper...)

The *Kp* index represents maximal variations within 3-hour time intervals. Any solar-wind parameter that will be correlated with it also has to have the same time resolution. Additionally to adapting the time resolution, we have to consider by which means it should be done. Simple 3-hour average values should have a lower correlation coefficient than the solar-wind parameter's 3-hourly maximal variation.

The 3-hour maximal variations are obviously higher when using high resolution data. Thus, to be able to correlate *Kp* with solar-wind data, high resolution data (e.g., 1 min) is needed to determine the maximal solar-wind variations within each 3-hour interval.

The longest time coverage has the hourly OMNI data set (since 1963), however we prefer to use the minutely OMNI data with the time range 1981–2016, to benefit from higer correlation

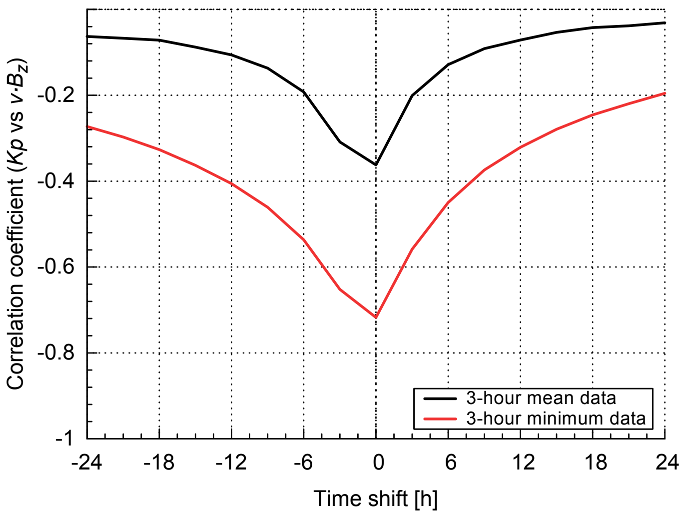

Fig. 7. Kp-vB_z correlation coefficients for different time shifts. Minutely OMNI data from 1981–2016 processed with mean (black) and minimum (red) 3-hour averaging.

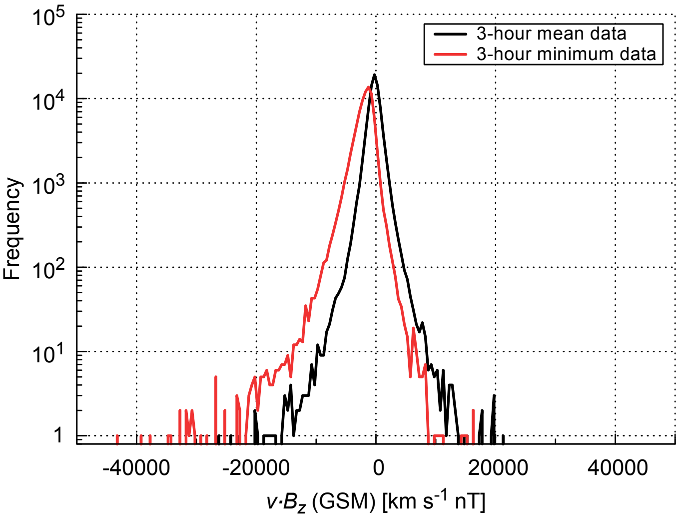

Fig. 8. Frequency distributions of vB_z for 3-hour mean (black) and minimum (red) minutely OMNI data from 1981–2016.

coefficients (see Figs?).

Pearson correlation coefficients; use Spearman rank instead? correlate positive and negative values separately?

Kp-vB_z Pearson correlation coefficients for mean and minimum, see Fig. 7.
The largest correlation is found for the 3-hour minimum data without time shift. It is a negative correlation with a coefficient of -0.72.

We use vB_z 3-hour minimum values, as a result their frequency distribution and its peak is asymmetrically shifted to negative values, as seen in Fig. 8.
even the 3-hour mean shows a slight offset in position (why?)

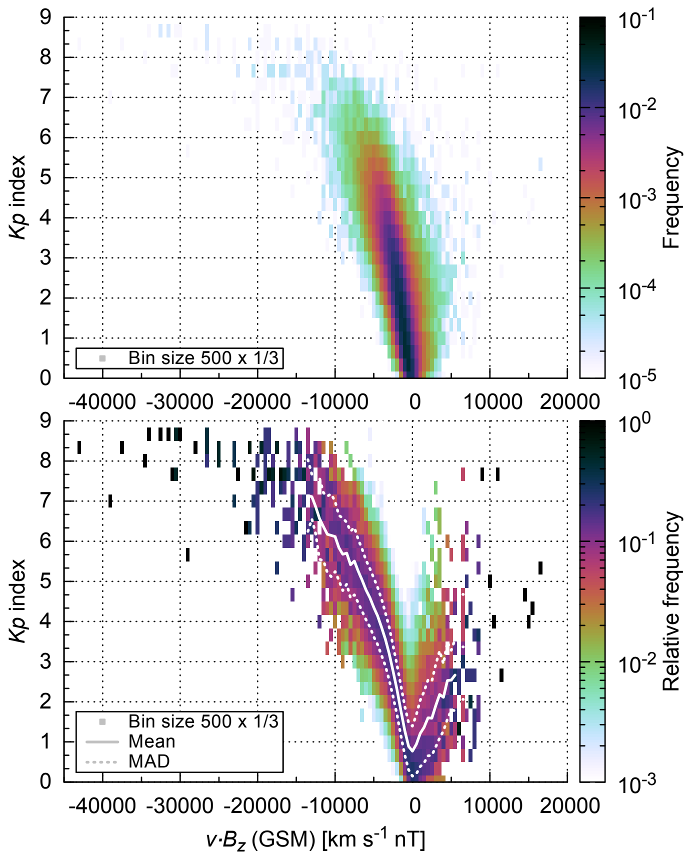

Fig. 9. Kp versus vB_z frequency distribution (top) and its relative distribution (bottom) with the mean Kp values (solid) and their mean absolute deviation (dotted). It is 3-hour minimum data from the minutely OMNI data set (1981–2016). The bin size is 500 km s^{-1} nT and $1/3$ Kp unit respectively.

3.3. Functional dependency

The frequency distribution over the Kp-vB_z space is shaped like a candle flame inclined to negative values by a light breeze, see top panel in Fig. 9.

To determine a functional dependency we look at the relative frequencies per vB_z-interval and their mean Kp values, which are plotted in the bottom panel of Fig. 9. The mean absolute deviation (MAD) of the mean has a mean size of 0.7 Kp units. This probability distribution is asymmetrically V-shaped around zero, having a larger and steeper negative arm. This effect is not a result of the data reducing method (3-hour minimum), because for 3-hour mean data the asymmetry also exists (fig...?). Rather the steeper negative arm is a consequence of the half-wave rectifier coupling of the solar-wind magnetic field direction to the magnetosphere as described in Sect (coupling section...).

Since the Kp index has a quasi-logarithmic scaling (see Basics...), a logarithmic function is the obvious choice as a fit function. Furthermore, the depending argument consists of a product of two solar-wind parameters which individually scale logarithmically with Kp. These reasons are why we use the logarithm of a parabola for the fitting approach:

$$f(x) = \ln(x^2)\,. \tag{4}$$

We introduce a horizontal shifting parameter $x2$ because the distribution's center is slightly offset. To be able to replicate the asymmetry in both arms, we split the fit function into a negative

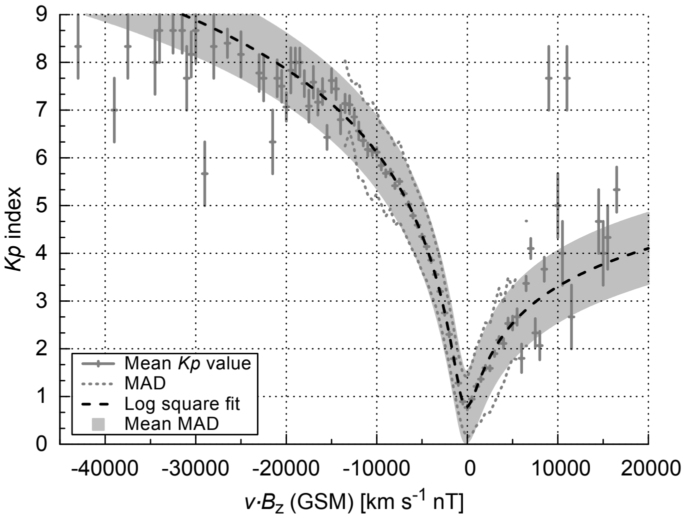

Fig. 10. Mean Kp values (+) and MAD values (dotted) per vB_z interval. The error bars represent the relative data count. The logarithmic fit (dashed) is plotted with a mean MAD band (shaded area). The splitted function (5) is used for the weighted fit. OMNI data from the time period 1981–2016 is used.

and a positive part:

$$f(x) = \begin{cases} f_-(x) & \text{for } x < 0\,, \\ f_+(x) & \text{for } x \geq 0\,. \end{cases} \tag{5}$$

This way both arms can be scaled individually with the scaling factors for the negative and positive parts a and c. The resulting logarithmic fit functions are

$$f_-(x) = a \cdot \ln((x + x2)^2 + d) + b\,, \tag{6}$$

$$f_+(x) = c \cdot (f_-(x) - f_-(-x2)) + f_-(-x2)\,, \tag{7}$$

with the vertical shifting parameter b and the depth parameter d.

The resulting fit is plotted in Fig. 10 with the fit coefficients $a = 1.258(19)$, $b = -17.04(33)$, $c = 0.467(20)$, $d = 1.416(68) \times 10^6$ and $x2 = 163(20)$ for units of [km s^{-1} nT].

Thus, the solar-wind dependency relation condenses to:

$$Kp_-(vB_z) = 1.26 \cdot \ln((vB_z + 160)^2 + 1.42 \times 10^6) - 17.0\,, \tag{8}$$

$$Kp_+(vB_z) = 0.47 \cdot (Kp_-(vB_z) - Kp_-(-160)) + Kp_-(-160)\,. \tag{9}$$

This relation can be used together with real-time in situ measurements from spacecraft located at L1 to nowcast the actual Kp index.

4. *Kp* forecast from remote CME observations

Compared to the steady solar wind, which can be measured reliably only from in situ measurements, CMEs can already be sighted raising from their source region on the solar surface. From remote coronagraph observations, some CME properties can be estimated and modeled to Earth, such as its propagation direction and its arrival time and arrival velocity (cites?). Thus, early observations enable a heads-up time only depending on the CME's propagation speed to Earth. This travel duration can be more than 4 days for slow events with average solar-wind speeds, about 40 hours for fast events with average speeds of 1000 km s^{-1}, and down to 20 hours and even below for the rare extreme cases, e.g., about 21 hours for the event on 23 July 2012 (Russell et al. 2013; Temmer & Nitta 2015) and about 19 hours for the event observed by Carrington (1859) on 1 September 1859.

To make use of the heads-up time for CMEs, we simplify the coupling relation (3) from before by neglecting its magnetic field part, which can hardly be determined from remote observations. Therefore, the only coupling parameter left is the solar-wind velocity.

4.1. *CME velocity estimation*

methods and modeling...?
GCS, CAD modeling -> propagation direction and apex height-time profile -> acceleration and velocity kinematics...
-> example event CME?

4.2. *SWS CME list*

For the following analysis we use the list of solar-wind structures (SWS) created and updated by Richardson et al. (2000); Richardson & Cane (2012), who characterized the near-Earth solar-wind structures since 1963. All periods related to ICMEs in the OMNI solar-wind data set were identified and flagged.

The SWS list for 1963–2016 was kindly provided by Ian Richardson (private communication). into acknowledgments...

SWS list for 1963–2015 by (Richardson et al. 2000; Richardson & Cane 2012) is available via registration at CEDARweb[6].
List of near-Earth ICMEs since January 1996 by Cane & Richardson (2003); Richardson & Cane (2010). Available as ACE Level 3 data for the period 1995–mid2016[7].

The CME fraction of the OMNI time series for the period 1981–2016 is 15.8 % (5.53 years) and that for the period 1963–2016 is 17.0 % (9.01 years).

4.3. *Data processing and correlation*

Again we calculate 3-hour extreme values using the minutely OMNI data to profit from higher correlation coefficients, like done for the data processing of the vB_z analysis in Sect. 3.2. For the velocity these are 3-hour maximum values. The comparison between the 3-hour maximum and the 3-hour mean frequency distributions show that their mean position raises from 405 to 425 km s^{-1}, see Fig. 11.

Using the CME periods from the SWS list as a filter, the CME part and non-CME part of the data can be examined separately. Their frequency distributions show that in faster solar

[6] CEDARweb website for Solar Wind Structures: `http://cedarweb.vsp.ucar.edu/wiki/index.php/Tools_and_Models:Solar_Wind_Structures` (existent in 2017-10-29)
[7] ACE Level 3 data website – list of near-Earth ICMEs: `http://www.srl.caltech.edu/ACE/ASC/DATA/level3/icmetable2.htm` (existent in 2017-10-29)

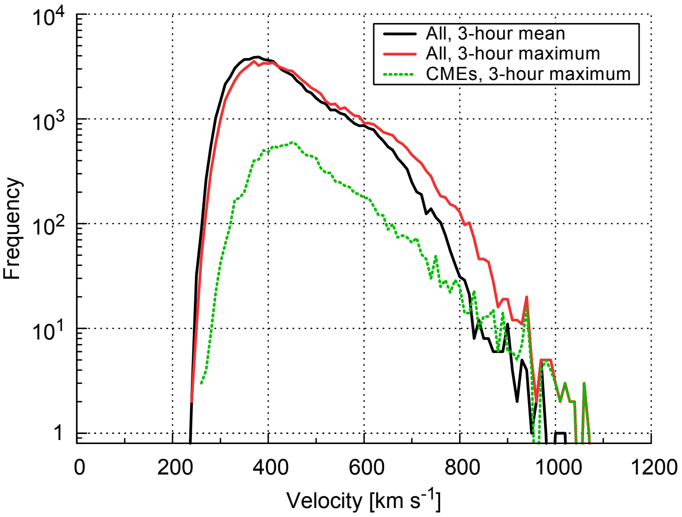

Fig. 11. Solar wind velocity frequency distributions for 3-hour mean (black), maximum (red) and maximum of the CME part (green). Minutely OMNI data from the period 1981–2016 is used.

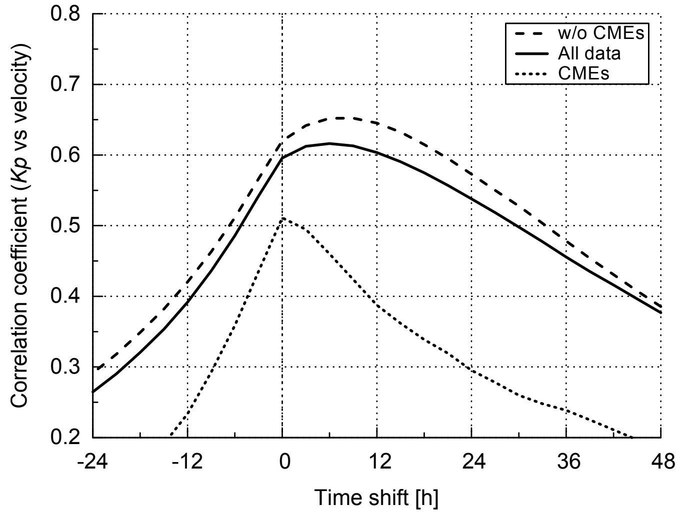

Fig. 12. *Kp*-velocity correlation coefficients for different time shifts. The correlations for the whole solar-wind data (solid), for solar wind without CMEs (dashed) and for CMEs only (dotted) are plotted. The used data is the 3-hour maximum of the minutely high resolution OMNI data.

wind the CME share is rising until eventually in the region above about 900 km s^{-1} there exist only CMEs, see Fig. 11.

The CME part of the data is correlated with the *Kp* index independently from the remaining solar wind, see Fig. 12. The correlation for CME related data is smaller than that for the regular solar wind. Its maximal correlation coefficient with a value of 0.51 is without time shift, see Table 1. The regular solar wind without CMEs shows a higher correlation with *Kp* and its maximal coefficient of 0.66 is at a positive time shift of 9 hours, that is, the *Kp* index forecasts the velocity of regular solar wind 9 hours in advance.

The positive time shift can be explained with the occurence of interaction regions followed by high speed streams (HSS). When a slow solar-wind stream is followed by a fast one, the compression at their interface leads to enhanced solar-wind densities and magnetic field strengths. The peak velocity of a HSS naturally appears after the interaction region. Therefore the *Kp*-impact of the enhanced magnetic field is correlated with the higher velocity of the HSS, yielding the observed positive time shift.

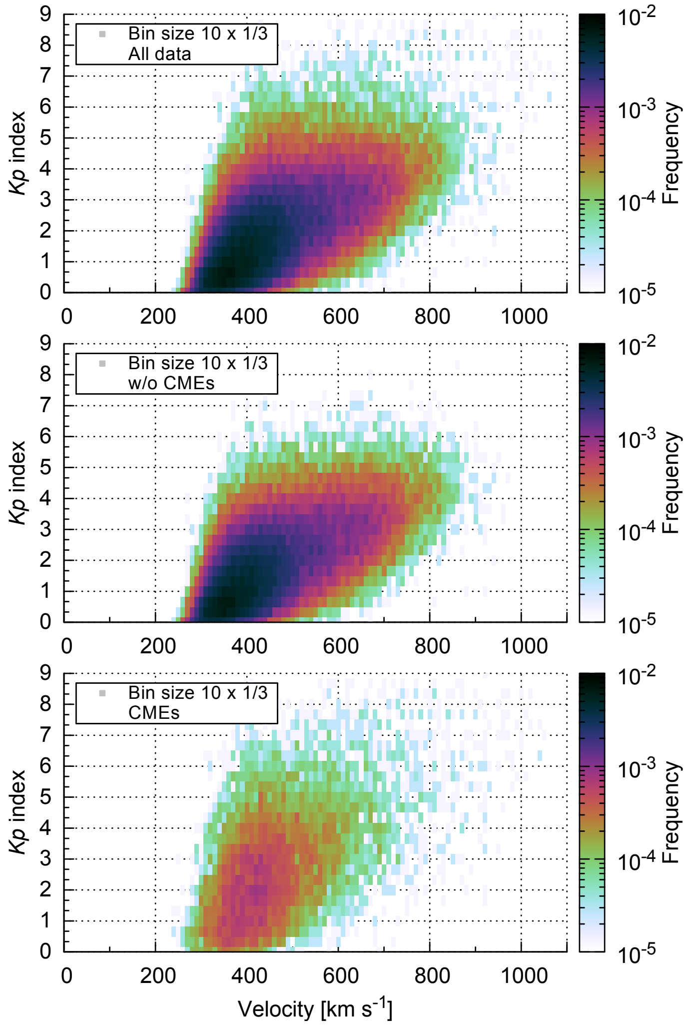

Fig. 13. *Kp*-velocity distributions for the whole solar-wind data, for solar wind without CMEs and for CMEs only. The used data is the 3-hour maximum of the minutely high resolution OMNI data. For the CME separation the SWS list from Richardson & Cane (2012) is used. The bin size is 10 km s^{-1} and 1/3 *Kp* unit respectively.

4.4. Functional dependency for CMEs

The general *Kp*-velocity dependency is apparent in the tilt of its distribution, see top panel of Fig. 13. The comparison with the CME data shows that *Kp* values > 7 and velocities > 900 km s^{-1} are almost always associated with CME related periods, see middle and bottom panel of Fig. 13.

To find a functional dependency for the mean *Kp* value we look at the relative frequencies per velocity interval, which are plotted in the bottom panel of Fig. 14. The mean *Kp* value seems to scale almost linear with the solar-wind velocity. The mean absolute deviation of the mean has a mean size of about 1.1 *Kp* units.

Again, as the *Kp* index has a quasi-logarithmic scaling, a logarithmic function is the obvious choice for the fitting process, for

Table 1. Time lags with the highest correlation coefficients for the *Kp*-velocity relation. The used data is the 3-hour maximum of the minutely high resolution OMNI data.

Data	Time lag [hours]	Correlation coefficient
All data	6	0.622
w/o CMEs	9	0.661
CMEs	0	0.511

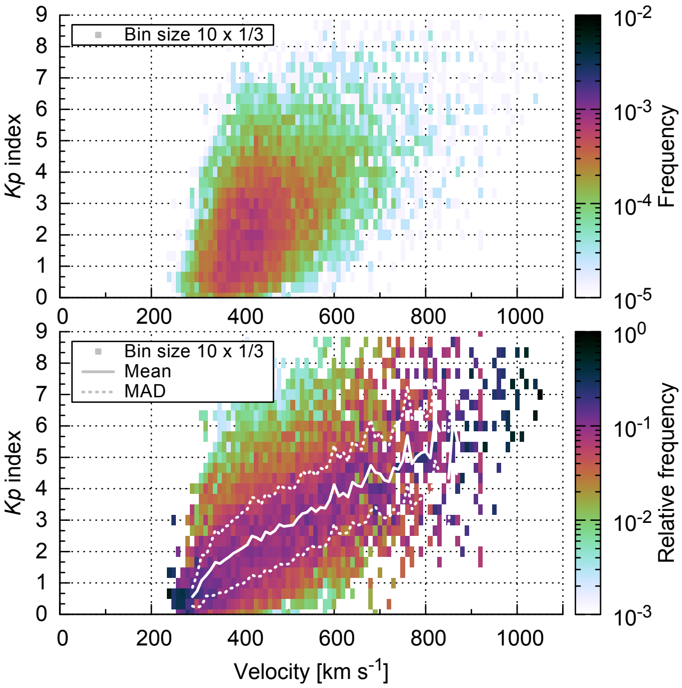

Fig. 14. CME part of the *Kp*-velocity distribution (same as third panel of Fig. 13) and its relative distribution per velocity interval with the mean *Kp* values (solid) and their mean absolute deviation (dotted). The bin size is $10\,\mathrm{km\,s^{-1}}$ and $1/3$ *Kp* unit respectively.

which thus the logarithmic function

$$f(x) = a \cdot \ln(x + x1) + b \tag{10}$$

is used, with the scaling factor a, the location parameter $x1$ and the vertical shifting parameter b.

The resulting fit is plotted in Fig. 15, with velocity in units of $[\mathrm{km\,s^{-1}}]$ its parameters are $a = 10.6(34)$, $b = -73(28)$ and $x1 = 8.1(43) \times 10^2$.
This leads to the CME dependency function

$$Kp(v) = 11 \cdot \ln(v + 800) - 70\,, \tag{11}$$

which can be used to forecast the *Kp* index from the estimated CME arrival velocity.

4.5. Functional dependency for non-CMEs

use of by 9-hours shifted data..., see Fig. 12

To find a functional dependency for the mean *Kp* value we look at the relative frequencies per velocity interval, which are plotted in the bottom panel of Fig. 16. The mean *Kp* value seems to scale almost linear with the solar-wind velocity. The mean absolute deviation of the mean has a mean size of about

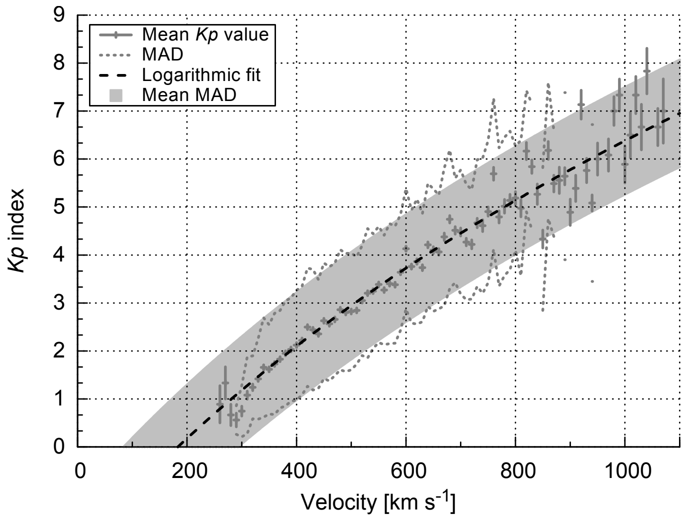

Fig. 15. Mean *Kp* values (+) and MAD values (dotted) per velocity interval for the CME part of the data. The error bars represent the relative data count. The logarithmic fit (dashed) is plotted with a mean MAD band (shaded area). The function (10) is used for the weighted fit. The CME part of the OMNI data from the period 1981–2016 is obtained using the SWS list from Richardson & Cane (2012).

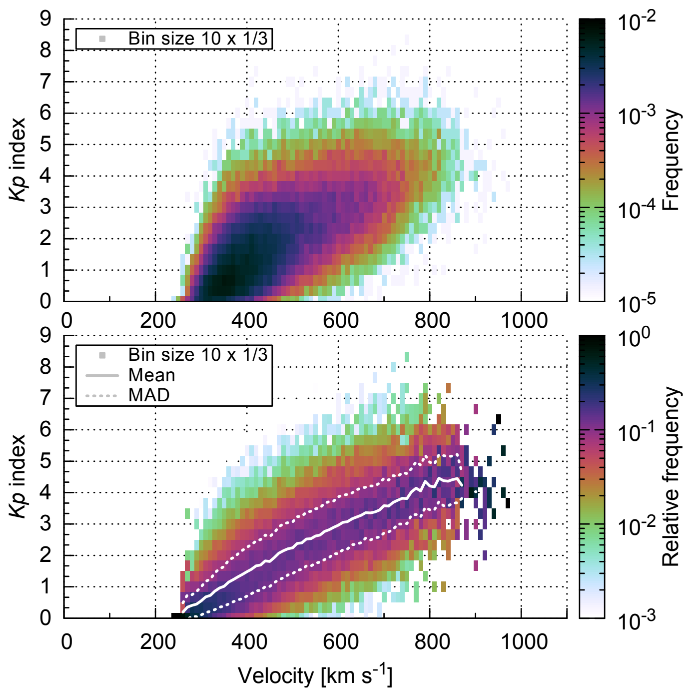

Fig. 16. Non-CME part of the *Kp*-velocity distribution (similar to second panel of Fig. 13, but with the by 9-hours shifted data) and its relative distribution per velocity interval with the mean *Kp* values (solid) and their mean absolute deviation (dotted). The bin size is $10\,\mathrm{km\,s^{-1}}$ and $1/3$ *Kp* unit respectively.

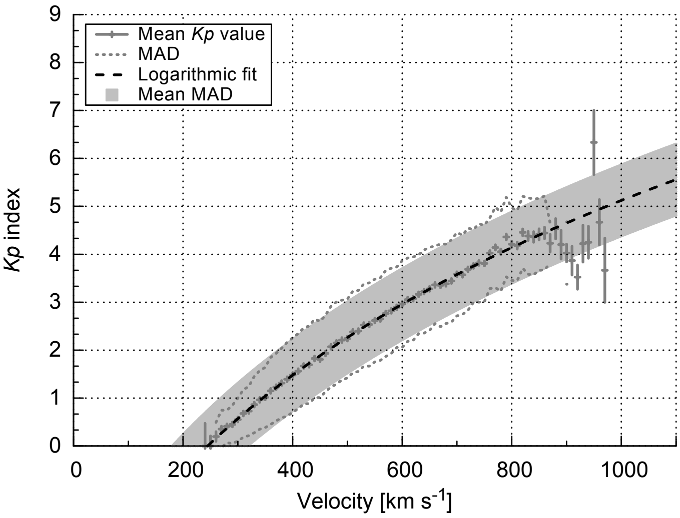

Fig. 17. Mean *Kp* values (+) and MAD values (dotted) per velocity interval for the non-CME part of the data, shifted by 9-hours. The error bars represent the relative data count. The logarithmic fit (dashed) is plotted with a mean MAD band (shaded area). The function (10) is used for the weighted fit. The non-CME part of the OMNI data from the period 1981–2016 is obtained using the SWS list from Richardson & Cane (2012).

0.7 *Kp* units.

Again, as the *Kp* index has a quasi-logarithmic scaling, a logarithmic function is the obvious choice for the fitting process, for which thus the logarithmic function (10) is used.

The resulting fit is plotted in Fig. 17 and the fit parameters are $a = 5.88(38)$, $b = -3.70(29) \times 10^1$ and $x1 = 2.99(49) \times 10^2$, with velocity in units of $[\mathrm{km\,s^{-1}}]$.
This leads to the non-CME dependency function

$$Kp(v) = 5.9 \cdot \ln(v + 300) - 37\,, \tag{12}$$

which can be used to forecast the *Kp* index from the estimated velocity coming from coronal hole analysis.

5. Results and discussion

solar activity: *Kp*-*ssn* relation
seasonal changes: *Kp*-month relation
solar-wind nowcast: Kp-vB_z relation (average and worst case)
CME forecast: *Kp*-velocity relation (average and worst case)
non-CME forecast: *Kp*-velocity relation (average and worst case)

Kp-velocity correlation
similar to Elliott et al. (2013); different data time period, resolution and averaging method (3-hour maximum of 1 min data)

6. Outlook

Applications:
Kp-rssfeed, realtime solar-wind and *Kp* plot
CME *Kp* impact (part of UGOE DDC)

scientists develop an advanced prototype space weather warning system to ensure the operation of telecommunication and navigation systems on Earth to the threat of solar storms

The prototype/precursor relations are integrated into applications developed within the Advanced Forecast For Ensuring Communications Through Space (AFFECTS) project which ran from 2011 to 2013. There are services accessible via the AFFECTS website[8].

list of services with *Kp* developed applications/implementations (all links existent in 2017-11-19):

- DSCOVR real-time solar-wind plot `http://www.affects-fp7.eu/rssfeeds/ace_ap_plot/ace_realtime_ap_plot.png`
- DSCOVR real-time solar-wind with Kp plot `http://www.affects-fp7.eu/rssfeeds/ace_ap_plot/ace_realtime_ap_plot.png`
- DSCOVR real-time solar-wind plot Kp forecast `http://www.affects-fp7.eu/rssfeeds/ace_ap_forecast_plot/ace_realtime_ap_CH_GFT_plot.png`
- RSS L1 SW Alert: `http://www.affects-fp7.eu/rssfeeds/rssfeed_sw/rssfeed_sw.xml`
- RSS L1 Kp Alert: `http://www.affects-fp7.eu/rssfeeds/rssfeed_kp/rssfeed_kp.xml`
- RSS L1 GNSS Alert: `http://www.affects-fp7.eu/rssfeeds/rssfeed_gnss/rssfeed_gnss.xml`
- RSS L1 Aurora Alert: `http://www.affects-fp7.eu/rssfeeds/rssfeed_aurora/rssfeed_aurora.xml`
- RSS L1 Aurora Alert (Kp 9): `http://www.affects-fp7.eu/rssfeeds/rssfeed_aurora_kp9/rssfeed_aurora.xml`
- iPhone app L1 Alerts (Solar wind latest 2-hour extreme values and derived forecast values): `http://www.affects-fp7.eu/app-services/L1-Alerts/dataL1Alerts.txt`
- Android app L1 Alerts...
- has SW-Display Kp forecast?
- CME *Kp* impact (part of UGOE DDC)
- Kp forecast calculation: `http://www.astro.physik.uni-goettingen.de/~mvenzmer/kp_forecast_calculation/kp_forecast_calculation.php`

mobile apps app store links?

reduce list to Kp-related apps...

Acknowledgements. The research leading to these results has received funding from the European Union's Seventh Framework Programme (FP7/2007-2013) under the grant agreement number 263506 (AFFECTS).
The authors thank the Helios and OMNI PIs/teams for creating and making available the solar wind in situ data. The OMNI data are supplied by the NASA Space Science Data Coordinated Archive (NSSDCA) and the Space Physics Data Facility (SPDF) at NASA's Goddard Space Flight Center (GSFC).
Additional thanks for maintaining and providing the international sunspot number series goes to the World Data Center – Sunspot Index and Long-term Solar Observations (WDC-SILSO) at the Solar Influences Data Analysis Center (SIDC), Royal Observatory of Belgium (ROB).
The hourly solar wind structure list was kindly provided by Ian Richardson of the NASA Goddard Space Flight Center and CRESST/University of Maryland via the CEDAR Database at the National Center for Atmospheric Research, which is supported by the National Science Foundation.
The results presented in this paper rely on the *Kp* index, calculated and made available by the German Research Centre for Geosciences in Potsdam from data

[8] AFFECTS website (existent in 2017-11-19): `http://www.affects-fp7.eu`

collected at magnetic observatories. We thank the involved national institutes, the INTERMAGNET network and ISGI (isgi.unistra.fr).

References

Bartels, J. 1962, Naturwissenschaften, 49, 313
Bothmer, V. 1993, PhD thesis, Georg-August-Universität Göttingen
Cane, H. V. & Richardson, I. G. 2003, Journal of Geophysical Research (Space Physics), 108, 1156
Carrington, R. C. 1859, MNRAS, 20, 13
Elliott, H. A., Jahn, J.-M., & McComas, D. J. 2013, Space Weather, 11, 339
Machol, J. L., Reinard, A. A., Viereck, R. A., & Biesecker, D. A. 2013, Space Weather, 11, 434
Richardson, I. G. & Cane, H. V. 2010, Sol. Phys., 264, 189
Richardson, I. G. & Cane, H. V. 2012, Journal of Space Weather and Space Climate, 2, A2
Richardson, I. G., Cliver, E. W., & Cane, H. V. 2000, J. Geophys. Res., 105, 18203
Rotter, T., Veronig, A. M., Temmer, M., & Vršnak, B. 2012, Sol. Phys., 281, 793
Russell, C. T. 2007, The coupling of the solar wind to the Earth's magnetosphere, ed. V. Bothmer & I. A. Daglis, 103
Russell, C. T., Mewaldt, R. A., Luhmann, J. G., et al. 2013, ApJ, 770, 38
Temmer, M. & Nitta, N. V. 2015, Sol. Phys., 290, 919
Vršnak, B., Temmer, M., & Veronig, A. M. 2007, Sol. Phys., 240, 315